



A novel lift controller for a wind turbine blade section using an active flow control device: experimental results

Loïc Michel, Ingrid Neunaber, Rishabh Mishra, Caroline Braud, Franck Plestan, Jean-Pierre Barbot, Pol Hamon

► To cite this version:

Loïc Michel, Ingrid Neunaber, Rishabh Mishra, Caroline Braud, Franck Plestan, et al.. A novel lift controller for a wind turbine blade section using an active flow control device: experimental results. The IEEE 2022 Conference on Control Technology and Applications (CCTA), Aug 2022, Trieste, Italy. hal-03787452

HAL Id: hal-03787452

<https://hal.science/hal-03787452>

Submitted on 26 Sep 2022

HAL is a multi-disciplinary open access archive for the deposit and dissemination of scientific research documents, whether they are published or not. The documents may come from teaching and research institutions in France or abroad, or from public or private research centers.

L'archive ouverte pluridisciplinaire **HAL**, est destinée au dépôt et à la diffusion de documents scientifiques de niveau recherche, publiés ou non, émanant des établissements d'enseignement et de recherche français ou étrangers, des laboratoires publics ou privés.

A novel lift controller for a wind turbine blade section using an active flow control device: experimental results

L. Michel¹, I. Neunaber², R. Mishra², C. Braud², F. Plestan¹, J.-P. Barbot^{1,3},
P. Hamon^{1,4}

Abstract—In this paper, a very recent adaptive version of super-twisting is applied to the control of the aerodynamic lift over wind turbine blades taking into account local disturbances of the air flow. The proposed control law acts as a model-free control strategy that is based on the definition of only two parameters. Thanks to this strategy, the tuning and modeling efforts are reduced: the first parameter is acting on the gain variation speed, whereas the second one is linked to the expected accuracy, thus allowing the control of unknown dynamics. The ability of the proposed control algorithm is discussed to track a lift reference for a wind turbine blade in presence of external perturbations. Experimental results globally illustrate the feasibility of such a control.

I. INTRODUCTION

Wind turbines are subjected to many disturbances (both atmospheric and mechanical) [1], which may, at least on average, be compensated by pitch control. Even if the pitch control [2] shows global efficiency, it is possible to improve the performances by using local aerodynamic controllers. Different types of local actuators (for example, flaps or plasma), which have been developed for control purposes, are associated with control algorithms sufficiently robust and act on the blade aerodynamics. Few contributions have been made so far.

A review on the control strategies dedicated to gust alleviation problems using active flow control, is proposed in [3] including modeling techniques [4], [5]. Feedback and feedforward structures [6] have been studied in the framework of a controlled wind turbine blade for active load reduction based on system identification [7] [8] [9] [10] [11]. A proportional controller has been proposed in [12] to reduce lift fluctuations in a constant shear inflow simulated by oscillations of a 2D blade section. Micro-jets have been successfully implemented as a fast control technology and are able to significantly dampen the lift oscillations; however, some lift fluctuations remain. The work of [12] has been improved by using a model-free control technique [13] ; this controller has been implemented by the authors [14] to control micro-jets installed at the trailing edge of a 2D blade section. The experimental test bench used to test the efficiency of this control in presence of turbulence includes a wind perturbation system described in Section II.

Extremum-seeking control (ESC), associated with sliding mode control [15] [16], has been implemented in the framework of aerodynamic drag reduction [17]. The ESC method has also been used as a real-time optimization strategy to cope with high-lift problems in the context of flow instability at the blade section scale through active flow control [18]. Alternatively, sliding mode control (SMC) [15] [16] is a robust nonlinear control approach that is particularly well suited to control perturbed uncertain nonlinear systems. However, due to its discontinuous feature, this class of control strategy generates the chattering phenomenon (high frequency oscillations). Several solutions have been proposed to attenuate this drawback; among them, one can firstly cite the concept of high order sliding mode control. This class of controllers allows to reduce the chattering, to keep the robustness and to improve the accuracy. One of the most famous high order sliding mode controllers is the super-twisting [19] that is a second order sliding mode algorithm; its main features being that it is a continuous output feedback. An other way to reduce the chattering is the dynamic adaptation of the controller gain: the simple idea is to adapt the controller gain with respect to the accuracy (the gain is increased if the accuracy is not sufficient whereas, when the targeted accuracy is reached, the gain is reduced). Numerous adaptation laws have been proposed for first [20], [21], [22], [23], [24], [25] or second order sliding mode controllers such that twisting [26], [27], [28] or super-twisting [29], [30], [31], [32] .

In this paper, the choice towards adaptive super-twisting algorithm has been made for several reasons: first-of-all, as previously recalled, this is a controller that is continuous and does not use time derivative of the sliding variable, reducing the chattering by an efficient way. Furthermore, there exist several adaptive versions of super-twisting, from the initial version [29] to very recent ones [33], [34], these latter using very few tuning parameters (for [34], two parameters as in [33] but with respect to six for [29]). Notice that this class of adaptive controllers require a very reduced knowledge of the system; only the fact that the uncertainties/perturbations are bounded and that the system can be locally modelled as a first order model.

In this experimental study, for the first time in aerodynamics, the adaptive super-twisting algorithm, proposed in [34], is used to control the lift using micro-jets. Notice that a model-free controller [14] has already been applied in this control application. The chosen super-twisting algorithm can be viewed as a model-free solution since no model is

¹Nantes Université, Ecole Centrale Nantes, CNRS, LS2N, UMR 6004, F-44000 Nantes, France. **Corresponding author:** Loïc Michel, loic.michel@ec-nantes.fr.

²Nantes Université, Ecole Centrale Nantes, CNRS, LHEEA, UMR 6598, F-44000 Nantes, France.

³ENSEA, Quartz Laboratory, EA 7393, F-95014, Cergy-Pontoise, France.

⁴ARMOR MECA Développement, F-22490, Pleslin-Trigavou, France.

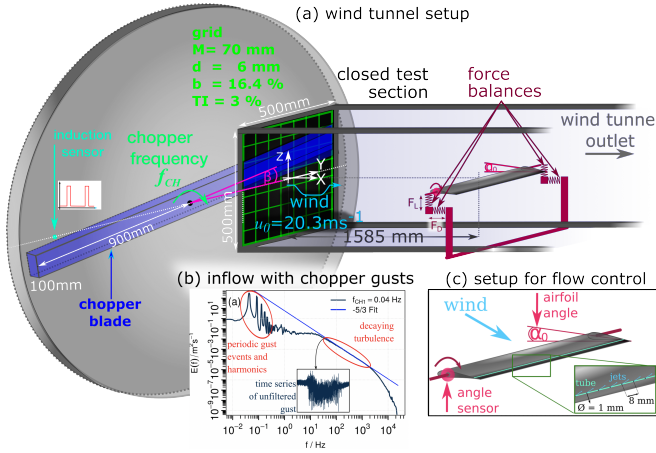


Fig. 1: (a) LHEEA aerodynamic wind tunnel: a gust generator, named “chopper”, can optionally be used. (b) Example of the energy spectrum of the flow generated by the chopper. (c) Setup used for active flow control measurements: a tube with holes is installed at the airfoil’s trailing edge and pressurized air is blown out of the holes.

required excepted the sign and minimum amplification of the link between the input-output. Moreover, only global aerodynamic force measurement is used as a feedback for the control.

The paper is structured as follows. Section II describes the experimental setup whereas Section III presents the adaptive super-twisting algorithm including its main properties. Section IV illustrates and analyses some experimental results.

II. EXPERIMENTAL SETUP

The experimental bench, detailed in the sequel, is composed of a wind tunnel with its perturbations system, a 2D aerodynamic blade profile equipped by micro-jets (for the lift control), and lift and drag sensors.

A. Wind tunnel facility and gust generator

The LHEEA aerodynamic wind tunnel is a recirculating one. The test section has a cross-section of $500 \times 500 \text{ mm}^2$ and a length of 2300mm (Figure 1). The turbulence intensity of an undisturbed inflow in the wind tunnel is around 0.3%. In the present study, a grid is installed at the inlet of the test section to generate turbulent inflow with a turbulence intensity of 3%. This bypasses the laminar-to-turbulent transition occurring at low Reynolds numbers and low angles of attack (AoA) for this blade geometry (see the linear part of the lift curve in Figure 2). The inlet of the test section is additionally equipped with a system which enables the generation of a sudden variation of the mean flow with turbulence superimposed on it. This system is called “chopper” and consists of a rotating bar that cuts through the inlet of the test section (Figure 1(a)). Figure 1(b) displays the energy spectrum of a gust produced by the chopper. In this work, however, the chopper is used in a static way by fixing its position in the inlet to add disturbances in the form of

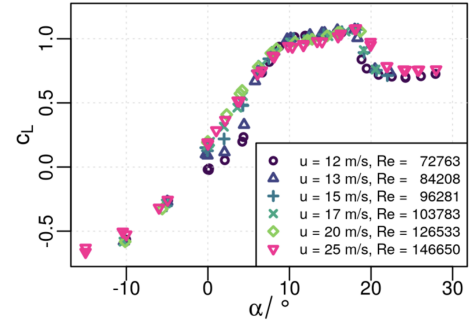


Fig. 2: Experimentally measured lift curves of the airfoil in dependence of the Reynolds number.

turbulent structures (in [14], the rotating chopper was used to produce a periodic reduction of the lift).

B. Aerodynamic profile

A 2D blade section of type NACA $65_4 - 421$ with a chord length of $c = 9.6 \text{ cm}$ is installed in the test section (Figure 5).¹ It is a thick profile with two changes of the lift curve corresponding to a first boundary layer separation at the trailing edge of the profile and a second flow separation at the leading edge, indicating stall (see [35] for more details on the blade aerodynamics). In the present study, the angle of incidence was set to $\alpha_0 = 20^\circ$ as preliminary open-loop tests have been found to produce control results easier to implement. Open-loop tests at angles of incidence of 0° , 10° and 20° have been performed to chose this angle of incidence (see Fig. 3). It can be shown that only a low control efficiency can be reached at 0° when the flow is still attached (i.e. maximum $\Delta F_L = 2.5 \text{ N}$). At 10° , the control efficiency is three times higher, but it is decreasing with the inlet pressure from $p = 1 \text{ bar}$. An angle of incidence of 20° is therefore chosen to ease the control implementation, as the control efficiency is still high with a linear increase with the inlet pressure. More investigations are needed to extend the present work to other angles of incidence.

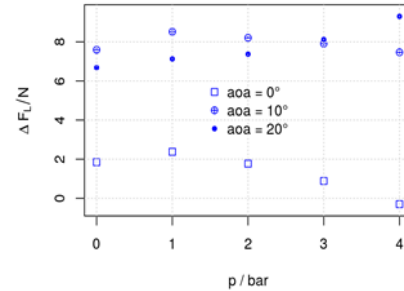


Fig. 3: ΔF_L versus pressure for different AoA.

¹Note that “2D blade section” here refers to a two-dimensional shape that is extruded in the third dimension so that the blade section spans the whole length of the wind tunnel.

C. Lift and drag measurements

Two sets of Z6FC3 HBM bending beam load cell sensors are used, and they are mounted on both sides of the 2D blade section support to measure the lift and drag forces. As shown in Figure 1(a), each set consists of two load cells mounted with in a 90° angle to measure the forces in the X (drag) and Z (lift) directions. They are calibrated *in situ* using gauge weights from 0 – 5 kg in steps of 0.5 kg.

D. Micro-jets

To control the flow around the airfoil, holes of 1 mm diameter with equidistant 8 mm spacing are placed at 1.92 cm from the airfoil's trailing edge, along the entire spanwise direction (Figure 1(c)). They are connected to a plenum chamber, itself fed with pressurized air at 6 bar. The air circuit is connected to solenoid valves that are acting as On/Off switches, so that pulsed micro-jets can be generated with a repetition rate of up to 300 Hz.

E. Control hardware

The control is managed by a STM32 Nucleo board H743ZI2 allowing a 16-bit ADC acquisition as well as the possibility to monitor the signals in real-time on the computer (Figure 4 presents the control hardware where the Nucleo board is mounted on a fully featured PCB): the lift force measured by the force balances is used as input signal. It is acquired with a sampling frequency of 20 kHz using the Nucleo board. The signal is filtered using a fourth order Butterworth filter with a cut-off frequency of 20 Hz. The control updates at 20 kHz and drives the valve at 200 Hz in response to the input from the force balances. As a consequence, the control of the system can be viewed as a duty-cycle.

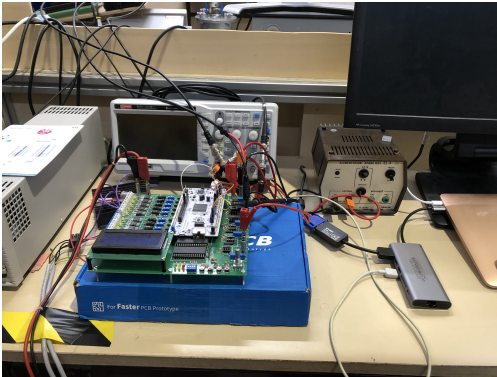


Fig. 4: Experimental setup within the wind tunnel : the board control.

Figure 5 displays a view of the experimental setup focusing on the wind tunnel, the measurement system and the air injection system.

III. ADAPTIVE SUPER-TWISTING BASED CONTROLLER DESIGN

A. Problem statement

The control objective is to ensure that the lift of the blade is tracking a reference in spite of the wind variations and

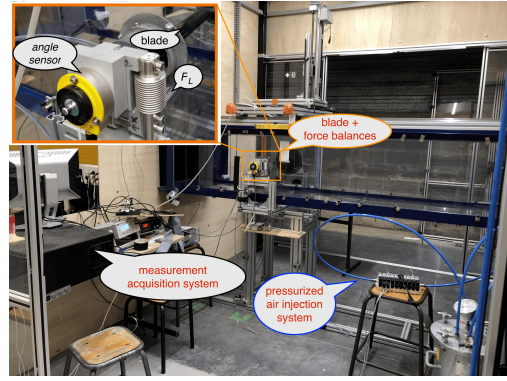


Fig. 5: Experimental setup: the wind tunnel test section with the 2D blade section, force balances, measurement acquisition, and pressurized air injection system.

turbulences, thanks to the action of the micro-jets. As shown in Fig. 6, the control signal drives the signal sent to the solenoid valves to release or block the pressurized air in front of the micro-jets on the airfoil surface. The measured lift is forced to a reference and the valve is driven using a variable duty-cycle (conversion of the output of the control as a PWM signal) at the constant frequency of 200 Hz.

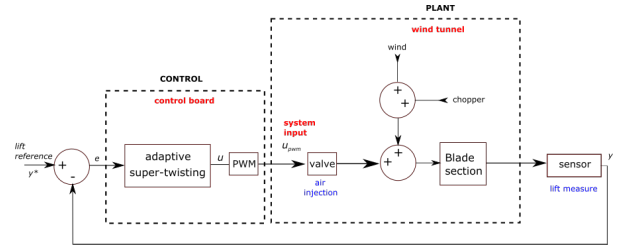


Fig. 6: Closed-loop scheme.

The blade lift control design is based on the following observation: the modeling of the studied system is a very hard task. Thus, control approach with a limited modeling process is considered. In such way, model-free controller [13] has been proposed in [14]: it is supposed that the relation between the micro-jets produced force and the lift force (see Figure 6) can be modelled by a first-order system. However, the robustness of such controller is not ensured. The current paper proposes an intrinsic adaptive robust controller based on second order sliding mode strategy [15].

B. A solution with limited knowledge of the system

Another solution consists in using an adaptive version of the super-twisting algorithm [34] given that

- it can be applied to a system with a relative degree equal to 1: that is the case given that, in previous work [14], the system has been viewed as a first-order system one;
- it does not require any modeling information (except the relative degree), its gain being dynamically adapted;
- it is intrinsically robust with respect to uncertainties and perturbation. Indeed, in such conditions, a real second order sliding mode [15] is established in finite time.

Defining the tracking error as σ such that $\sigma = y - y^*$ with y the measured lift and y^* the reference, from [14], the relation between σ and the control input u that is applied to the PWM system controlling the servo-valves, can be viewed as a perturbed first-order system with unknown static gain k and constant time τ under a perturbation $\delta(t)$, that is

$$\dot{\sigma} = -\frac{1}{\tau}\sigma + \frac{k}{\tau}u + \delta(t) \quad (1)$$

Supposing that parameters k and τ are constant but unknown, system (1) can be written as

$$\dot{\sigma} = a(\sigma, t) + b \cdot u \quad (2)$$

with $a(\sigma, t) = -\frac{1}{\tau}\sigma + \delta(t)$ and $b = \frac{k}{\tau}$. One supposes that both the function $a(\sigma, t)$ is bounded in the operating domain. Notice that, in sliding mode context, the variable σ is called “sliding variable”. Moreover, $-\frac{1}{\tau}\sigma$ is a dissipative term that contributes to the boundedness of $a(\sigma, t)$.

Given that b is supposed constant (but unknown), system (2) has a similar form than the class of systems considered in [34]. From [34], the adaptive super-twisting controller reading as

$$\begin{aligned} u &= -k_1 |\sigma|^{\frac{1}{2}} \text{sgn}(\sigma) + v \\ \dot{v} &= -k_2 \text{sgn}(\sigma) \end{aligned} \quad (3)$$

with the adaptive rules of the gains k_1 et k_2 :

$$\dot{k}_1 = \begin{cases} \frac{\alpha}{|\psi| + \epsilon} & \text{if } |\sigma| > \epsilon \\ -k_1 & \text{if } |\sigma| \leq \epsilon \end{cases} \quad (4)$$

$$\dot{k}_2 = \begin{cases} \frac{\alpha}{2|\sigma|^{\frac{1}{2}}} & \text{if } |\sigma| > \epsilon \\ -k_2 & \text{if } |\sigma| \leq \epsilon \end{cases} \quad (5)$$

with $\psi = -\hat{\sigma}$, $\alpha > 0$ and $\epsilon > 0$ constant parameters; $\hat{\sigma}$ is the numerical estimation of $\dot{\sigma}$, that allows the stabilization of system (2) around the origin in a finite time.

For the seek of implementation simplicity, the numerical estimation of $\hat{\sigma}$ is performed using the basic Euler method. The gains k_1 and k_2 are adjusted based on the proposed adaptation laws (4)-(5). The adaptation protocol drives the evolution of the gains k_1 and k_2 according to the value of σ . The main ideas behind the adaptation rules are the following

- if $|\sigma| > \epsilon$, it can be due to the fact that the gains are not sufficient with respect to the effects of the perturbations and uncertainties (recall that a and b in (2) are unknown, a being bounded and b constant). So, the gains are increased (as displayed by first equations of (4)-(5)) as long as the desired accuracy is achieved, the parameter ϵ adjusting this accuracy target;
- if $|\sigma| < \epsilon$, the accuracy target is reached. The gains can be supposed to be enough with respect to the perturbations and uncertainties. So, the gains can be reduced as displayed by the gains dynamics (second equations of (4)-(5)). When the gains become too small or if a larger perturbation/uncertainty appears, the accuracy can be lost; the previous item is then considered and so on.

Since the convergence zone depends on the parameter ϵ , it is necessary to chose it sufficiently small to ensure the accuracy of the closed-loop system; however, it is necessary to tune it at a sufficient value in order to take into account the sampling period effect (see Section 4 of [20] for the relation between the accuracy target ϵ and the sampling period). The parameter α is acting on the dynamics of adaptive gains and should be chosen according to an initial estimation of the “magnitude” of the open-loop dynamic response of the system including an estimation of the perturbation².

IV. EXPERIMENTAL RESULTS

The experiments are conducted considering a constant inflow velocity of 20.3 ms^{-1} , measured with a Pitot static tube above the airfoil in the undisturbed flow, and an angle of incidence of the 2D blade section of 20° . The chopper can create a reduction of the air flow and is used to evaluate the robustness of the proposed adaptive super-twisting control under perturbations of the lift.

The efficiency of the lift tracking is evaluated for several scenarios. In each scenario, the tracking of the lift is presented according to the evolution of the duty-cycle and the evolution of the gains k_1 and k_2 .

- **Scenario 1: external static perturbations while starting the control.** Figures 7, 8 and 9 illustrate the open-loop behavior of the lift force without air injection, then the reference tracking of the closed-loop system considering piece-wisely constant changes of the reference. A constant (turbulent) perturbation induced by the fixed chopper is applied during all the scenario.
- **Scenario 2: wind speed change and perturbation during the control.** Figures 10, 11 and 12 illustrate the tracking of the lift considering piece-wisely constant changes of the reference under changes of the wind speed as well as the introduction of a perturbation while the control is running.

The parameters of the adaptive super-twisting controller are set to $\alpha = 7000$ and $\epsilon = 0.1$ whereas the initial values of both gains are $k_1(0) = k_2(0) = 10$. Remark that in the different study cases, with respect to such kind of active flow control, the range of α (resp. ϵ) is between 5000 and 8000 (resp. 0.05 and 0.5).

In Scenario 1, the wind speed is initially set to 20.3 ms^{-1} . Using a fixed position of the chopper blade, a perturbation is introduced at the beginning of the test performed to set the lift values in the open-loop. Then, the control starts at $t = 31 \text{ s}$ and a transient of the adaptation of the gains k_1 and k_2 is observed that allows the lift to reach the targeted reference (see Figure 7). The control allows to efficiently track the lift reference in spite of the perturbation: the gains k_1 and k_2 (see Figure 8) quickly increase because the lift is lower due to the perturbation. The effort requested to

²Notice that current works are made in order to remove the tuning process of ϵ and α , thanks to an online tuning process of both these parameters.

maintain the tracking efficient depends on the reference and the perturbation; as a consequence, a lower reference at $t = 63$ s may decrease the gains k_1 and k_2 despite the constant perturbation (see Figures 7 and 8).

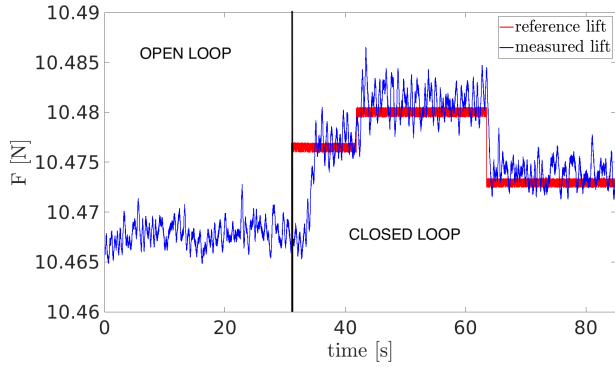


Fig. 7: **Scenario 1:** Measured lift and reference lift versus time (sec).

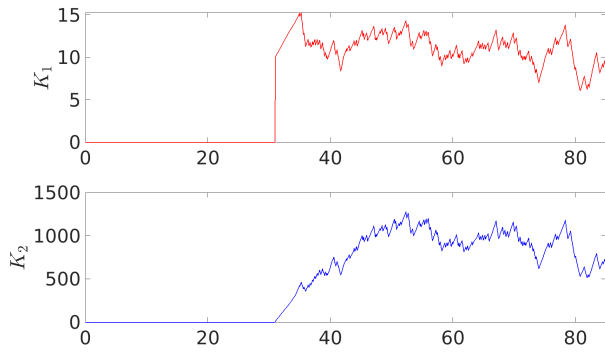


Fig. 8: **Scenario 1:** Gains k_1 and k_2 versus time (sec).

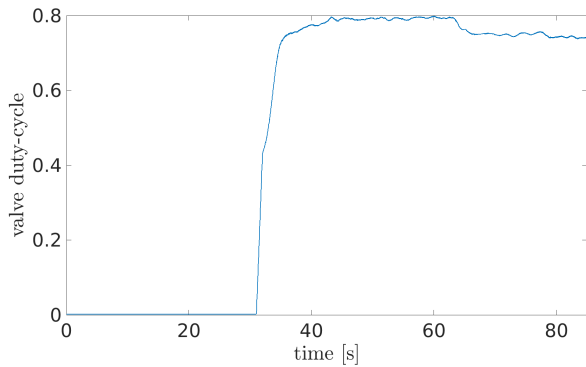


Fig. 9: **Scenario 1:** Duty-cycle versus time (sec).

In Scenario 2, the wind speed is initially set to 20.3 ms^{-1} and no perturbation is introduced at the initial time. The wind speed is modified at $t = 12$ s. A perturbation is introduced by moving the chopper blade into the inlet at $t = 50$ s and is increased at $t = 60$ s (by moving the

chopper blade further into the inlet, thus further decreasing the wind velocity). The control reacts to the changes of the lift induced by the wind velocity variations to ensure a satisfying tracking. Accordingly, the reaction of the control can be seen both through the value of the duty-cycle (Figure 12) that is adjusted when perturbations occur and through the adaptation of k_1 and k_2 (Figure 11) that are increased while the perturbations occur. In particular, at $t = 60$ s, the perturbation increases thus inducing an additional decrease of the lift, for which the gains are adapted again to higher values. The turbulence has a greater impact than the reference variations in parameters k_1 and k_2 .

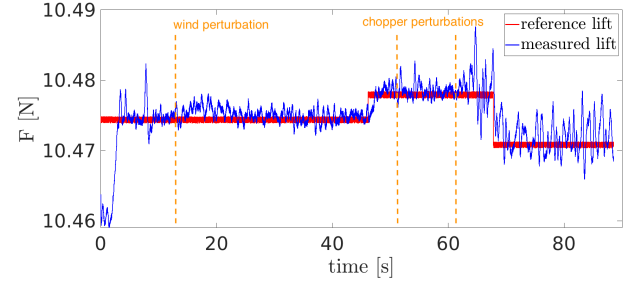


Fig. 10: **Scenario 2:** Measured lift and reference lift versus time (sec).

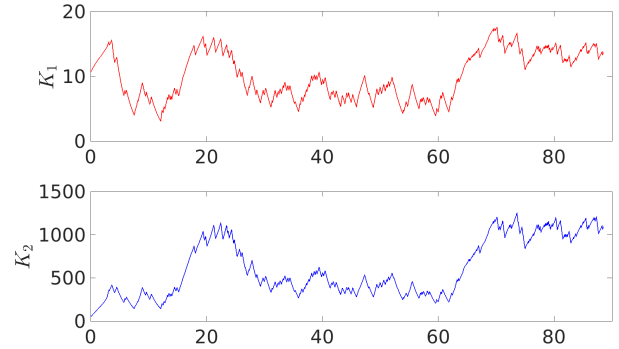


Fig. 11: **Scenario 2:** Gains k_1 and k_2 versus time (sec).

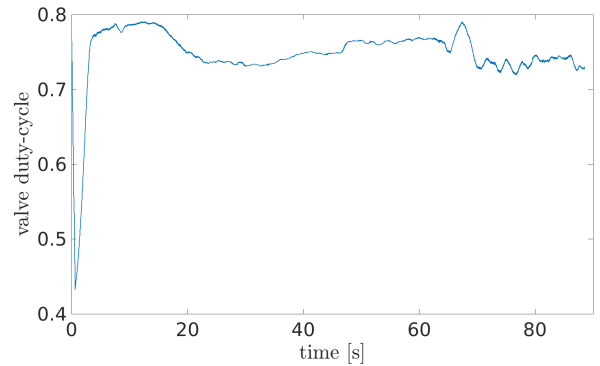


Fig. 12: **Scenario 2:** Duty-cycle versus time (sec).

According to the adaptation rules, the gains are dynam-

ically increased while a perturbation is disturbing the lift (either the wind speed or the static chopper) to compensate the perturbation and to maintain the tracking. When starting the control, a certain transient is needed to start the adaptation of the gain in order to set the initial tracking of the lift (see Figures 10 and 7).

Remark: the rejection of the high frequency perturbations can be managed differently considering another choice of α , ϵ , k_1 and k_2 in (4) and (5). Moreover, the high frequency perturbations are, to the best of knowledge, also due to the limitations of the dynamic of the micro-jets and measurement noise.

V. CONCLUSIONS

An adaptive super-twisting based control of the lift force acting on an airfoil by using and controlling micro-jets has been designed and experimented. Different scenarios of experimental tests have been carried out to illustrate the robustness of the control. Promising results show that satisfying tracking performances have been obtained despite the perturbations.

Future investigations will be focused on the lift control design combining the use of blade pitch and the use of micro-jets.

ACKNOWLEDGMENTS

The authors thank Dr. Pierre Molinaro for the design of the electronic control board in the experimental setup. This work is supported by *Agence Nationale de la Recherche* (ANR) with project CREATIF ANR-20-CE05-0039.

REFERENCES

- [1] J.G. Schepers et al. Technical report, IEA Wind TCP Task 29, Phase IV: Detailed Aerodynamics of Wind Turbines, may 2021.
- [2] Ervin Bossanyi. The design of closed loop controllers for wind turbines. *Wind Energy*, 3:149–163, 2000.
- [3] David R. Williams and Rudibert King. Alleviating unsteady aerodynamic loads with closed-loop flow control. *AIAA Journal*, 56(6):2194–2207, 2018.
- [4] B. G. Allan, J. Juang, D. L. Raney, A. Seifert, L. G. Pack, and D. E. Brown. Closed-loop separation control using oscillatory flow excitation. Technical report, NASA/CR-2000-210324, ICASE Report 2000-32, 2000.
- [5] Nailu Li and Mark J. Balas. Aeroelastic control of wind turbine blade using trailing-edge flap. *Wind Engineering*, 38(5):549–560, 2014.
- [6] S. Bartholomay et al. Pressure-based lift estimation and its application to feedforward load control employing trailing-edge flaps. *Wind Energy Science*, 6(1):221–245, 2021.
- [7] Thanasis Barlas, Jan Willem van Wingerden, Anton Hulskamp, and Gijs van Kuik. Closed-loop control wind tunnel tests on an adaptive wind turbine blade for load reduction. In *46th AIAA Aerospace Sciences Meeting and Exhibit*, 2008.
- [8] T. Shaqarin, C. Braud, and S. Coudert. Open and closed-loop experiments to identify the separated flow dynamics of a thick t.b.l. *Experiment in fluids*, 54(1448), 2013.
- [9] Nailu Li and Mark J. Balas. Adaptive flow control of wind turbine blade using microtabs with unsteady aerodynamic loads. In *2013 IEEE Green Technologies Conference (GreenTech)*, pages 134–139, 2013.
- [10] T. Shaqarin. Active control to reattach a thick turbulent boundary layer. PhD thesis, Ecole Centrale Lille, France, Nov. 2011.
- [11] R. Becker, M. Garwon, C. Gutknecht, G. Barwolf, and R. King. Robust control of separated shear flows in simulation and experiment. *J. of Process Control*, 15:691–700, 2005.
- [12] V. Jaunet and C. Braud. Experiments on lift dynamics and feedback control of a wind turbine blade section. *Renewable Energy*, 126:65–78, 2018.
- [13] M. Fliess and C. Join. Model-free control. *International Journal of Control*, 86(12):2228–2252, 2013.
- [14] L. Michel, I. Neunaber, R. Mishra, C. Braud, F. Plestan, J.P. Barbot, X. Boucher, C. Join, and M. Fliess. Model-free control of the dynamic lift on a wind turbine blade section: experimental results. In *Proceedings of TORQUE'22*, accepted.
- [15] Y. Shtessel, C. Edwards, L. Fridman, and A. Levant. *Sliding Mode Control and Observation*. Springer, New York, USA, 2014.
- [16] Vadim Utkin and Hao-Chi Chang. Sliding mode control on electro-mechanical systems. *Mathematical Problems in Engineering*, 8, 2002.
- [17] K. Mariette. *Contrôle en boucle fermée pour la réduction active de traînée aérodynamique des véhicules*. PhD thesis, INSA of Lyon, France., Nov. 2020.
- [18] R. Becker, R. King, R. Petz, and W. Nitsche. Adaptive closed-loop separation control on a high-lift configuration using extremum seeking. *AIAA Journal*, 45(6):1382–1392, 2007.
- [19] A. Levant. Sliding order and sliding accuracy in sliding mode control. *International Journal of Control*, 58(6):1247–1463, 1993.
- [20] F. Plestan, Y. Shtessel, V. Brégeault, and A. Poznyak. New methodologies for adaptive sliding mode control. *International Journal of Control*, 83(9):1907–1919, 2010.
- [21] G. Bartolini, A. Levant, F. Plestan, M. Taleb, and E. Punta. Adaptation of sliding modes. *IMA Journal of Mathematical Control and Information*, 30(3):285–300, 2013.
- [22] L. Hsu, T. Oliveira, J. Paulo, V. Cunha, and L. Yan. Adaptive unit vector control of multivariable systems using monitoring functions. *International Journal on Robust and Nonlinear Control*, 29(3):583–600, 2019.
- [23] S. Roy, S. Baldi, and L. Fridman. On adaptive sliding mode control without a priori bounded uncertainty. *Automatica*, 11, 2020.
- [24] L. Lin, Z. Liu, Y. Kao, and R. Xu. Adaptation of sliding modes. *IET Control Theory & Applications*, 14(3):519–525, 2020.
- [25] H. Obeid, L. Fridman, S. Laghrouche, and M. Harmouche. Barrier function-based adaptive sliding mode control. *Automatica*, 93:540–544, 2018.
- [26] Y. Shtessel, J. Moreno, and L. Fridman. Twisting sliding mode control with adaptation: Lyapunov design, methodology and application. *Automatica*, 75:229–235, 2017.
- [27] G. Liu, A. Zinober, Y. Shtessel, and Q. Niu. Twisting sliding mode control with adaptation: Lyapunov design, methodology and application. *Australian Journal of Electrical and Electronics Engineering*, 9(3):217–224, 2012.
- [28] M. Taleb, A. Levant, and F. Plestan. Electropneumatic actuator control: solutions based on adaptive twisting algorithm and experimentation. *Control Engineering Practice*, 21(5):727–736, 2013.
- [29] Y. Shtessel, M. Taleb, and F. Plestan. A novel adaptive-gain super-twisting sliding mode controller: methodology and application. *Automatica*, 48(5):759–769, 2012.
- [30] C. Edwards and Y. Shtessel. A novel adaptive-gain super-twisting sliding mode controller: methodology and application. *International Journal of Control*, 89(9):1759–1766, 2016.
- [31] V. Utkin and A. Poznyak. Adaptive sliding mode control with application to super-twist algorithm: Equivalent control method. *Automatica*, 49(1):39–47, 2013.
- [32] H. Obeid, S. Laghrouche, L. Fridman, Y. Chitour, and M. Harmouche. Barrier function-based adaptive super-twisting controller. *IEEE Transactions on Automatic Control*, 65(11):4928–4933, 2020.
- [33] S.V. Gutierrez, J. de Léon-Morales, F. Plestan, and A. Salas Pena. A simplified version of adaptive super-twisting control. *International Journal of Robust and Nonlinear Control*, 29(16):5704–5719, 2019.
- [34] F. Plestan and M. Taleb. Adaptive supertwisting controller with reduced set of parameters. In *2021 European Control Conference (ECC)*, pages 2627–2632, 2021.
- [35] A. Soulier, C. Braud, D. Voisin, and B. Podvin. Low-Reynolds-number investigations on the ability of the strip of tell-tale sensor to detect flow features over wind turbine blades: flow separation/reattachment dynamics. *Wind Energy Science*, 6:409–426, 2021.